Available online at www.sciencedirect.com
ScienceDirect
Trans. Nonferrous Met. Soc. China 35(2025) 3852−3868
Transactions of Nonferrous Metals Society of China
www.tnmsc.cn

Enhanced inhibition of chalcopyrite in molybdenite flotation by combined oxidation of microwave and H_2O_2

Ji-wei XUE, Qi-hong LIU, Tong LIU, He WAN, Sen WANG, Xian-zhong BU

School of Resources Engineering, Xi'an University of Architecture and Technology, Xi'an 710055, China

Received 29 February 2024; accepted 19 November 2024

Abstract: The effects of combined microwave and hydrogen peroxide (H_2O_2) oxidation on the flotation separation of molybdenite and chalcopyrite, as well as the underlying mechanism were investigated via microflotation, zeta potential, contact angle, X-ray photoelectron spectroscopy (XPS), scanning electron microscopy (SEM) and atomic force microscopy (AFM) analyses. The microflotation experiments showed that the effective inhibition of chalcopyrite can be obtained through combined oxidation pretreatments with low microwave power and H_2O_2 consumption. The zeta potential, contact angle and XPS analyses indicated that the surface hydrophobicity of molybdenite changed minimally after different treatments, whereas significant amounts of hydrophilic oxidation species were formed on the surface of chalcopyrite, thus decreasing its surface hydrophobicity and floatability. Moreover, the SEM and AFM analyses indicated that more uniform oxidative products were formed on the chalcopyrite surface, further significantly increasing the surface roughness.

Key words: molybdenite; chalcopyrite; flotation separation; combined oxidation; surface roughness

1 Introduction

As an important industrial raw material, molybdenum is widely used in various fields, such as steel, petroleum, chemicals, electrical and electronic technology, medicine and agriculture [1−3]. Molybdenum is primarily extracted from molybdenite, and flotation is one of the most commonly used methods for molybdenite recovery [4,5]. Molybdenite exhibits good natural floatability and can be easily obtained by adding hydrocarbon oil collectors, such as kerosene [6,7]. However, most of molybdenite is closely associated with chalcopyrite. Therefore, the effective depression of chalcopyrite in molybdenite flotation is crucial for obtaining high-quality molybdenum concentrates.

The floatability of chalcopyrite is similar to that of molybdenite, and the separation of these two minerals can be achieved by adding an inhibitor to suppress the flotation of chalcopyrite [8,9]. The inhibitors used in this process primarily include inorganic reagents (e.g., sodium sulfide, cyanide and Nokes agents) and organic reagents (e.g., sodium thioglycolate, thiocarbamides and polysaccharides). Sodium sulfide and sodium thioglycolate are currently the most commonly used inhibitors of chalcopyrite flotation and are widely used in industrial production. However, sodium sulfide is easily oxidized and loses its efficacy, thus rendering the flotation indicators unstable. Additionally, the use of sodium sulfide is disadvantageous to the environment and human health. Compared with sodium sulfide, sodium thioglycolate offers good inhibitory effects to chalcopyrite flotation and is less harmful to the environment. However, owing to oxidation, the inhibitory effects of sodium thioglycolate are weakened at high temperatures. In

Corresponding author: Xian-zhong BU, Tel: +86-18192833797, E-mail: buxianzhong@xauat.edu.cn
https://doi.org/10.1016/S1003-6326(25)66917-2

recent years, numerous studies have focused on the development of new types of organic inhibitors, such as thiocarbonohydrazide, tiopronin, 4-amino-5-mercapto-1,2,4-triazole, L-cysteine and tragacanth gum, which have been successfully applied for the effective inhibition of chalcopyrite flotation in small laboratories [10−14]. However, the complex production processes and high production costs limit their large-scale use in industrial production.

Different oxidation pretreatment techniques have been widely used, which were developed based on the different surface oxidation characteristics of chalcopyrite and molybdenite. Adding oxidants to render the surface of chalcopyrite selectively hydrophilic is a commonly used pretreatment technique. Hydrogen peroxide (H_2O_2) is typically used as an oxidant, and it has been widely used for the flotation separation of copper–molybdenum (Cu–Mo) minerals. However, to depress chalcopyrite effectively, a significant amount of H_2O_2 and a long pretreatment time are required. Thus, Fe^{2+} is typically introduced to enhance the inhibitory effects of H_2O_2. SUYANTARA et al [15] showed that Cu−Mo concentrate was successfully separated after being pretreated by H_2O_2 for 4.5 h. However, after adding H_2O_2 and Fe^{2+}, the pretreatment time was reduced to 5 min because of the strong oxidizing property of hydroxyl radical (·OH) which was generated by the reaction of H_2O_2 and Fe^{2+} [16]. The use of other oxidants, such as ozone (O_3), sodium hypochlorite (NaClO), ferrate (VI) and their combination, in the selective depression of chalcopyrite has been widely reported in the literatures [17−22]. However, these oxidants, particularly combination inhibitors, can corrode the equipment used.

Microwave oxidation is another oxidation pretreatment method. Under microwave irradiation, electromagnetic energy can be fully adsorbed by minerals and converted into thermal energy, thus promoting the surface oxidation of the minerals [23,24]. In addition, microwaves can effectively and selectively transfer heat, intensify the vibrations of polar molecules, and promote the overall heating of minerals. SILVA et al [23] demonstrated that microwave irradiation decreased the floatability of chalcopyrite by forming non-uniform oxidation or patched layers, and that flotation was restored by increasing the collector dosage. However, oxidation by microwave irradiation is weak unless the microwave power and pretreatment time are increased.

Therefore, the role of microwave oxidation in the flotation separation of chalcopyrite and molybdenite must be investigated comprehensively. In addition, studies regarding the effects of the combined oxidation of microwaves and H_2O_2 on the flotation separation of Cu−Mo minerals have not been reported. Therefore, in this study, the effects of combined oxidation pretreatment on the flotation separation of chalcopyrite and molybdenite were investigated, and the underlying mechanism was revealed via zeta potential measurements, contact angle measurements, X-ray photoelectron spectroscopy (XPS), scanning electron microscopy (SEM), and atomic force microscopy (AFM) analyses.

2 Experimental

2.1 Materials and reagents

Pure molybdenite and chalcopyrite samples were obtained from Guilin, Guangxi, China. The samples were crushed, manually selected, ground in quartz sand bowls and screened using a standard sieve to obtain samples of different sizes. Samples measuring −74 + 38 μm were used for microflotation and contact angle tests, as well as SEM and XPS measurements, and samples measuring −38 μm were prepared for zeta potential measurements. X-ray diffraction (XRD) and chemical elemental analyses were performed to determine the mineral composition of chalcopyrite and molybdenite (see Fig. 1 and Table 1). Based on the results of XRD analysis and chemical elemental analysis, the purity of chalcopyrite and molybdenite is 93.68% and 94.68%, respectively.

Analytical grade NaOH and HCl solutions were used to regulate the pulp pH, and H_2O_2 was used as the oxidant. Industrial grade emulsified diesel and terpenic oils were used as the collector and frother, respectively. During emulsification, the mass ratio of diesel-to-water was controlled at 1∶10. Meanwhile, polyoxyethylene lauryl ether was used as the emulsifier, which constituted 1.5% of the total mass of oil and water. Emulsified diesel was obtained after the mixture was treated for 2 min using an ultrasonic homogenizer (JY92-IIDN, NingBo Scientz Biotechnology Co., Ltd., China) with an ultrasonic power 300 W. Deionized (DI) water with a resistivity of 18.3 MΩ·cm was used for all the tests.

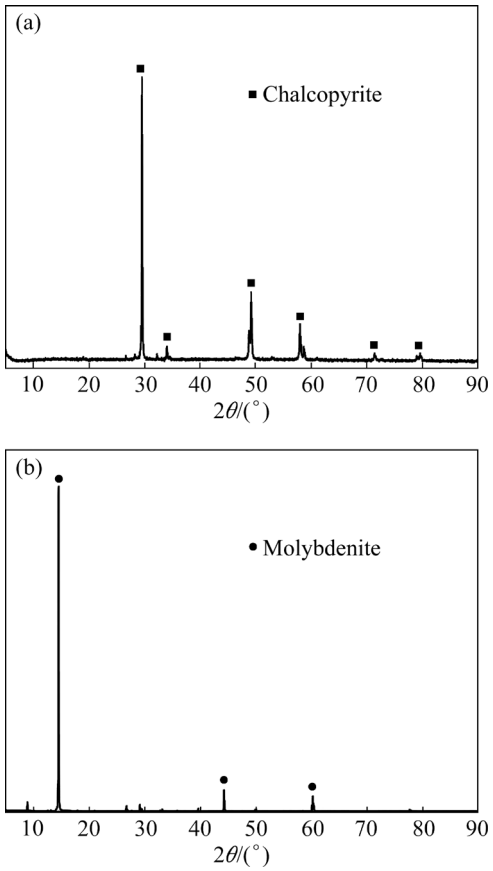

Fig. 1 XRD patterns of chalcopyrite (a) and molybdenite (b)

Table 1 Chemical elemental analysis results (%, mole fraction)

Sample	Cu	Mo	S	TFe	SiO_2
Chalcopyrite	32.44	−	29.52	33.16	0.53
Molybdenite	−	56.75	38.15	1.22	0.18

2.2 Oxidation pretreatments

Microwave pretreatment was performed in a CY-PY1100C-S microwave equipment. During oxidation, the sample was put in a ceramic crucible and then placed in the center of the cavity for pretreatment. During pretreatment, the microwave power was selected as the main variable.

Before H_2O_2 pretreatment, the samples with and without microwave pretreatment were blended with DI water in a beaker, and then the pH value was adjusted. Subsequently, diluted H_2O_2 was added to the solution and magnetically stirred at 500 r/min for a definite duration. After completing the pretreatments, the pulp was transferred into the flotation cell for the subsequent microflotation experiments.

To avoid the interference of natural oxidation on the subsequent oxidation pretreatments of the samples by microwaves and H_2O_2, the samples were blended with DI water in a beaker and then ultrasonicated for 5 min at a power of 100 W before oxidation.

2.3 Microflotation experiments

Microflotation tests were implemented using an XFD/FGC flotator (Jilin Prospecting Machinery Factory, China) with a rotation speed of 1800 r/min. Before flotation, 2 g of the sample was blended with 40 mL of DI water in the flotation cell. After adjustment for 4 min, NaOH or HCl, the collector and the frother were placed in consecutively and agitated for 3, 3 and 1 min, respectively. Finally, after floating for 4 min, the froth products and samples remaining at the bottom of the cell were obtained. The recovery rate of single minerals was calculated using Eq. (1). The productivity (γ) and recovery rate (ε) of the artificial mixture minerals were calculated using Eqs. (1) and (2), respectively [25].

$$\gamma=\frac{m_1}{m_1+m_2}\times 100\% \tag{1}$$

$$\varepsilon=\frac{\gamma\beta}{\alpha}\times 100\% \tag{2}$$

where m_1 and m_2 represent the mass of froth products and tailings, respectively, α and β represent the grade of the raw minerals and froth products, respectively.

2.4 Zeta potential measurements

The zeta potential of the samples after undergoing various pretreatments was measured using a JS94H analyzer (Shanghai Zhongchen Digital Technology Instrument Co., Ltd., China). For each measurement, 20 mg of the samples were blended with 40 mL of DI water in a beaker, then the KNO_3 solution with a concentration of 1×10^{-3} mol/L was added to maintain the ionic strength. After stirring the solution for 3 min, the pH value was adjusted and the solution was agitated for another 10 min. After the mixture was settled for 5 min, the appropriate solution was squeezed out and placed in an electrophoresis cell for measurement.

2.5 Contact angle measurements

The contact angles of chalcopyrite and

molybdenite after undergoing various pretreatments were determined using the pressing method. After the pretreatments and vacuum-dry, the samples were compressed into flakes with highly smooth surfaces and then subjected to contact angle measurements using a JC2000A contact angle measuring instrument (Shanghai Zhongchen Digital Technology Instrument Co., Ltd., China). After adjusting the focal length and position parameters, the droplets were extruded onto the surface of samples using a microsyringe, and images were obtained using a high-speed magnification camera to capture the moment of contact between the droplets and samples. The contact angle of each sample was measured using the angle-measuring method. The temperature of each measurement was maintained at approximately 25 °C.

2.6 XPS measurements

The samples used for XPS analysis were prepared based on the oxidation pretreatments. Then, the samples were rinsed, filtered and dried. XPS measurements were performed using a Thermo-Scientific ESCALAB 250X1 spectrometer. The instrument used an AlK_{α} X-ray source with a working voltage and current of 12.5 kV and 16 mA, respectively. The vacuum pressure in the analytical chamber was 8.0×10^{-7} Pa. After scanning all the elements, the related high-resolution spectra were obtained to analyze their valence and oxidation states on the surface of the samples. The collected peaks were fitted and analyzed using Thermo Avantage 5.979 software. The binding energy measured in these tests was compared to the standard C1s peak (284.8 eV) [26].

2.7 SEM measurements

The mineral surface morphologies of the samples subjected to different pretreatments were examined using a GeminiSEM500 field-emission SEM (Zeiss, USA). The highest resolutions of the secondary electron image by the equipment were 0.5 and 0.9 nm; the acceleration voltage was adjusted within the range of 0.02−30 kV; and the probe current was 3 pA−20 nA. During the test, the samples were cleaned ultrasonically and then oxidized under different conditions. After drying at a low temperature in a vacuum oven, the SEM images of the samples were obtained.

2.8 AFM measurements

The surface roughness of the samples subjected to different pretreatments was determined using AFM (Bruker, Germany). To obtain extremely smooth and flat surfaces, the block samples were polished using a 5000-mesh sandpaper. After the polished block samples were pretreated, the surfaces were dried using a nitrogen jet and used for measurements. The samples were scanned based on a procedure reported in Ref. [27], and the surface information of the samples was obtained by actuating the miniscule probe of the instrument across the surface of the samples. During the measurements, the surfaces were scanned under ambient air at an average temperature of (20.1±1.5) °C and relative humidity of (43.8±7.5)% using a Si_3N_4 gold-plated cantilever beam (SN-AF 01-S-NT, Epolied, Japan) with a spring constant of 0.08 N/m and a resonant frequency of 34 kHz. Subsequently, the surface roughness of the samples subjected to different treatments, as represented by the arithmetic average (R_a) value, was obtained using Eq. (3), and the corresponding averages were calculated [28]. The AFM measurement results were analyzed using the Nanoscope software.

$$R_a=\frac{1}{(L_xL_y)}\int_0^{L_y}\int_0^{L_x}|f(x,y)|\,\mathrm{d}x\mathrm{d}y \tag{3}$$

where $f(x, y)$ represents the surface relative to the central plane, and L_x and L_y represent different dimensions of the surface.

3 Results and discussion

3.1 Microflotation experiments

To investigate the effect of single and combined pretreatment methods on the flotation of chalcopyrite and molybdenite, microflotation experiments were performed under different conditions. The recoveries of chalcopyrite and molybdenite as a function of pH are shown in Fig. 2. As shown, the flotation of molybdenite was not impeded by the use of the single microwave or H_2O_2 pretreatment method, and its recovery remained above 88% in the measured pH range. Even after treatment was performed using the combined methods, the recovery of molybdenite decreased only slightly. This indicates that molybdenite is oxidized difficultly, which is consistent with the findings of previous studies [29,30]. However, the

flotation of chalcopyrite is sensitive to the oxidation pretreatment method in the measured pH range. After treatment with microwaves only, the recovery of chalcopyrite first increased from 65.14% to 70.27% when the pH value increased from 4 to 8. However, the recovery of chalcopyrite decreased gradually as the pH value increased further. When the pH value increased to 12, the recovery of chalcopyrite decreased to 55.17% owing to the enhancement in surface oxidation under strong alkaline conditions [31]. After treatment with H_2O_2 only, the recovery of chalcopyrite decreased in the pH range of 6−10 compared with the treatment by microwaves only. However, the recovery further increased when the pH value was 12, thus indicating H_2O_2 decomposition and efficacy loss due to the significant amounts of OH^- under strong alkaline conditions [32]. However, after treatment using the combined method, the recovery of chalcopyrite decreased significantly to less than 42.83% over the entire pH range. When the pH value was 10, the recovery of chalcopyrite was only 29.33%.

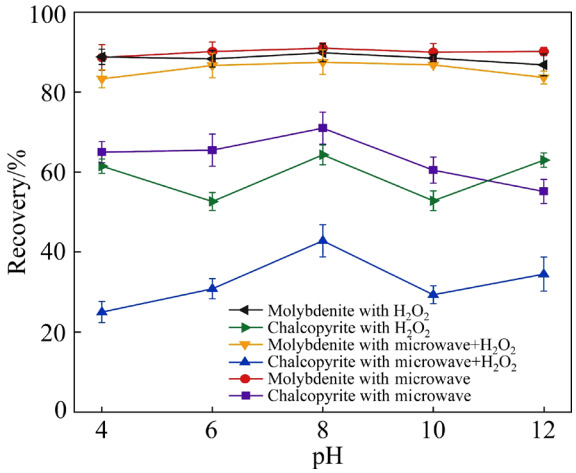

Fig. 2 Effect of pH on flotation recoveries of chalcopyrite and molybdenite with various pretreatments (H_2O_2 dosage 3.2×10^{-3} mol/L, microwave power 500 W)

The effect of H_2O_2 dosage on the flotation recoveries of chalcopyrite and molybdenite under different conditions is presented in Fig. 3. As shown, the recovery of molybdenite remained approximately 88% as the H_2O_2 dosage increased when the molybdenite was treated with the single and combined methods. Meanwhile, the recovery of chalcopyrite decreased gradually as the H_2O_2 dosage increased. After treatment with H_2O_2 only, the recovery of chalcopyrite decreased significantly from 71.83% to 36.67% when the H_2O_2 dosage increased from 1.1×10^{-3} mol/L to 9.7×10^{-3} mol/L. This indicates that high-dosage H_2O_2 facilitates the inhibition of chalcopyrite. However, after treatment with the combined method, the recovery of chalcopyrite was significantly lower than that afforded by the single treatment. When the H_2O_2 dosage increased from 1.1×10^{-3} to 3.2×10^{-3} mol/L, the recovery of chalcopyrite decreased from 42.64% to 25.13%. Subsequently, the recovery changed minimally as the H_2O_2 dosage increased further. Therefore, chalcopyrite was inhibited significantly when using the combined method with a H_2O_2 dosage of 3.2×10^{-3} mol/L.

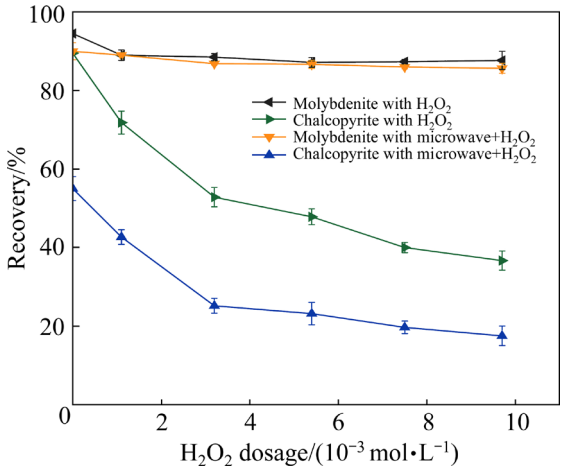

Fig. 3 Effect of H_2O_2 dosage on flotation recoveries of chalcopyrite and molybdenite with various pretreatments (pH=10, microwave power 500 W)

The effect of microwave power on the flotation of chalcopyrite and molybdenite under different conditions is presented in Fig. 4. As shown, after the single treatment, the recovery of molybdenite remained almost unchanged, whereas the recovery of chalcopyrite decreased gradually as the microwave power increased. When the microwave power increased from 100 to 1000 W, the recovery of chalcopyrite decreased significantly from 86.17% to 48.92%. However, after treatment with the combined method, the recovery of chalcopyrite decreased from 38.55% to 20.33% when the microwave power increased from 100 to 500 W. Subsequently, the recovery changed minimally as the microwave power increased further. Meanwhile, the recovery of chalcopyrite after treatment with the combined method was significantly lower than that afforded by the single treatment.

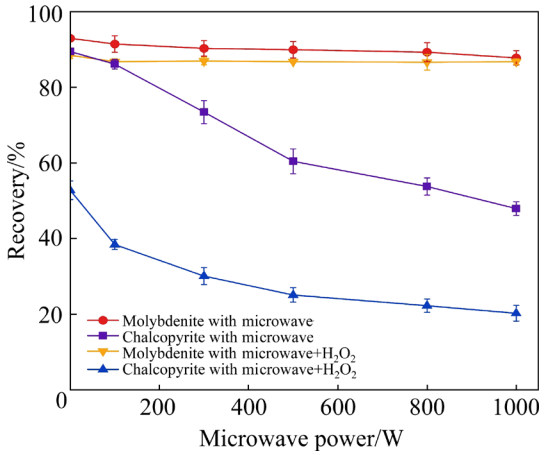

Fig. 4 Effect of microwave power on chalcopyrite and molybdenite flotation recoveries with various pretreatments (pH=10, H_2O_2 dosage 3.2×10^{-3} mol/L)

In conclusion, molybdenite is oxidized difficulty after treatment with single or combined methods. Furthermore, it can maintain good floatability under different conditions. Meanwhile, chalcopyrite is highly resistant to natural oxidation. However, after treatment with sufficient oxidation intensity, deep oxidation on chalcopyrite surface was observed. In particular, after treatment using the combined method, the recovery of chalcopyrite was extremely low. Therefore, the combined method is better than the single method for realizing the effective inhibition of chalcopyrite flotation and it can potentially achieve the flotation separation of chalcopyrite from molybdenite.

The results for the flotation test of artificial mixed minerals are presented in Fig. 5. As shown, for the samples without oxidation pretreatment, the grades of Cu and Mo in the concentrate were 18.77% and 29.07%, respectively. Additionally, the recovery of Cu and Mo was both above 80%, thus indicating the unsatisfactory flotation separation of chalcopyrite and molybdenite owing to the similar natural floatability of two minerals. After treatment with the single method, the grade of Cu decreased to less than 16%. However, the recovery of Cu exceeded 60% in the concentrate. Subsequently, when the mixed minerals were treated with the combined method, the grade and recovery of Cu decreased significantly to 3.36% and 10.80%, respectively. Meanwhile, a high-quality molybdenum concentrate was obtained with a grade and recovery of 54.88% and 97.70%, respectively. In conclusion, the inhibitory effect of the combined method on chalcopyrite flotation was better than that of the single method. During the flotation separation of Cu–Mo minerals, the flotation of chalcopyrite was effectively suppressed, and a high-quality molybdenum concentrate was obtained via the combined method involving microwaves and H_2O_2.

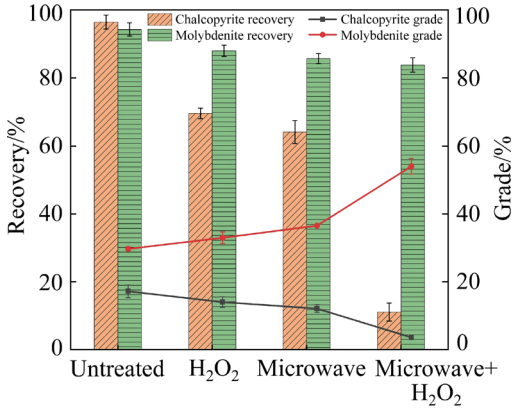

Fig. 5 Flotation separation of artificial mixed minerals with and without oxidation pretreatments (pH=10, microwave power 500 W, H_2O_2 dosage 3.2×10^{-3} mol/L)

3.2 Zeta potential analysis

The zeta potentials of chalcopyrite and molybdenite after different oxidation pretreatments are presented in Fig. 6. As shown, the zeta potential of untreated chalcopyrite decreased gradually with increasing pH, and the isoelectric point (IEP) was at pH<3. This indicated that chalcopyrite surface was not oxidized without pretreatments, which was consistent with the previously reported values in the literatures [23,33]. When chalcopyrite was treated with microwaves only, the zeta potential increased significantly in the measured pH range, and the IEP increased to pH 5.70. This indicated that when chalcopyrite was treated with microwaves, a mixture of copper and ferric oxides or hydroxides was generated on the surface. In addition, the surface solubility increased owing to oxidation, and numerous metal ions such as Cu^{2+} and Fe^{3+} dissolved in the solution. Subsequently, the positively charged ions and hydrolyzed species, such as $CuOH^+$, $Fe(OH)^{2+}$ and $Fe(OH)_2^+$, adsorbed onto the surface, thus causing the zeta potential to change positively in the measured pH range. When chalcopyrite was treated with the combined method, the zeta potentials were higher than that when it was treated with microwaves only in the measured pH range, while the IEP increased to pH 8.30. This indicated

that the oxidation on chalcopyrite surface was promoted and more oxidation products were generated on the surface.

Meanwhile, the IEP of molybdenite at pH<2 is presented in Fig. 6(b), which shows that the surface is negatively charged in the measured pH range. In addition, the zeta potential of molybdenite increases slightly after treatment with the single and combined methods in the pH range of 6−10, which is attributed to the generation of molybdenum oxides on the surface. Furthermore, the results confirm that molybdenite is oxidized difficultly. In conclusion, after oxidation pretreatment, the zeta potential of chalcopyrite increased significantly, whereas that of molybdenite changed slightly. Therefore, the oxidation of chalcopyrite due to the application of the combined method was significantly stronger than that of molybdenite.

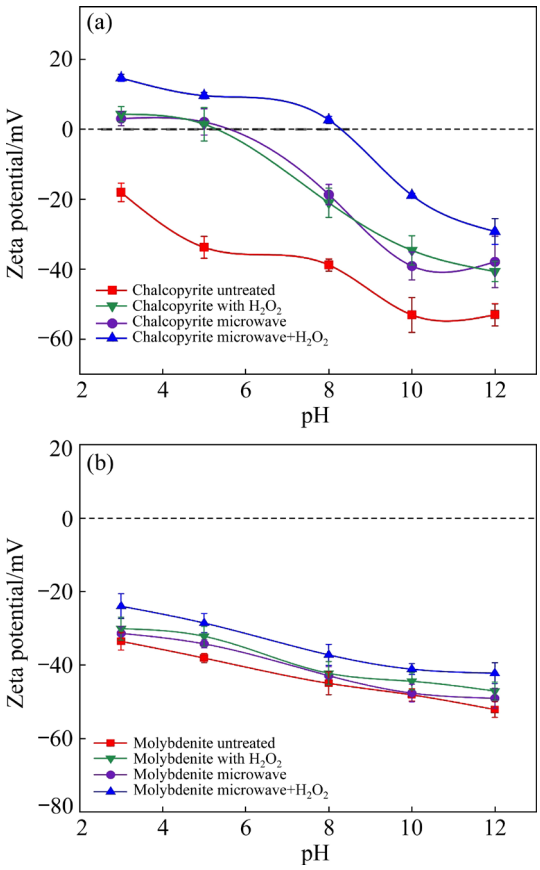

Fig. 6 Zeta potentials of chalcopyrite (a) and molybdenite (b) as function of pH (microwave power 500 W, H_2O_2 dosage 3.2×10^{-3} mol/L)

3.3 Contact angle measurements

The floatability of minerals can be evaluated from the change in the contact angles of the surface. As shown in Fig. 7, the contact angle of the untreated chalcopyrite and molybdenite was 81.54° and 84.56°, respectively. These values are consistent with those reported in the literatures and indicate that these two minerals exhibit good and similar natural floatability [34,35]. For molybdenite, the contact angle remained almost unchanged when the single and combined methods were used, thus indicating that it did not oxidize easily. However, for chalcopyrite, the surface wettability was sensitive to variations in the oxidation method. After microwave treatment, the contact angle of chalcopyrite decreased gradually as the microwave power increased. When the microwave power increased from 100 to 800 W, the contact angle of chalcopyrite decreased from 71.53° to 49.89°. As the microwave power increased further, the contact angle remained almost unchanged. This indicates that improving the surface wettability via microwave pretreatment alone is difficult. Therefore, the recovery of chalcopyrite remained higher than 50% even when the microwave power exceeded 800 W. However, after treatment with the combined method, the contact angle of chalcopyrite decreased

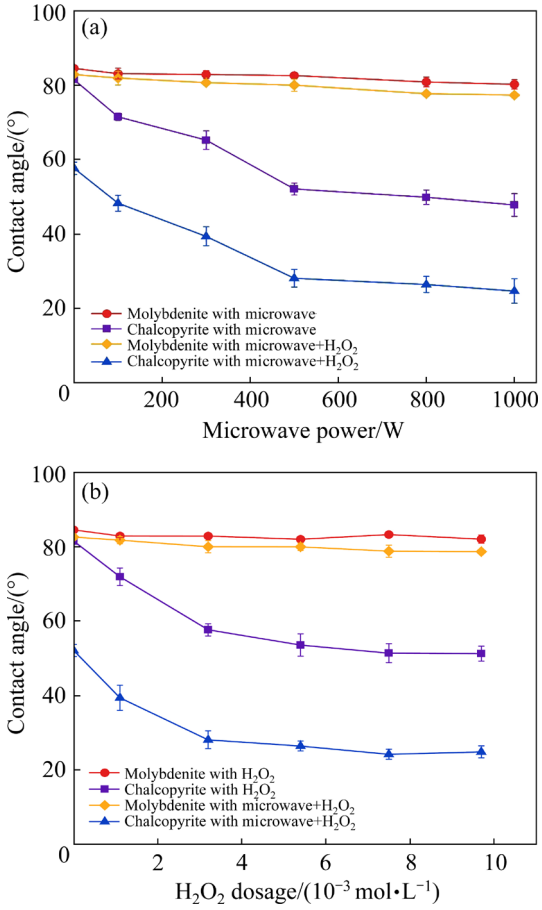

Fig. 7 Contact angles of chalcopyrite and molybdenite as functions of microwave power (a) and H_2O_2 dosage (b) after different pretreatments

significantly to less than 40° when the microwave power exceeded 300 W. This indicated that adding more H_2O_2 significantly improved the surface wettability and decreased the floatability of chalcopyrite.

As shown in Fig. 7(b), the single H_2O_2 pretreatment exerted a more profound effect on improving the wettability than the single microwave pretreatment. When the H_2O_2 dosage increased from 1.1×10^{-3} to 7.5×10^{-3} mol/L, the contact angle of chalcopyrite decreased rapidly from 71.93° to 51.40°, thus indicating that significant amounts of hydrophilic oxidation products were generated on the surface. When chalcopyrite was treated with the combined method, the contact angle further decreased as the H_2O_2 dosage increased. When the H_2O_2 dosage increased to 3.2×10^{-3} mol/L, the contact angle decreased significantly to 39.39°. Combining the findings above with the results shown in Fig. 7(a), it can be concluded that the combined method is more effective in decreasing the surface hydrophobicity of chalcopyrite. Therefore, chalcopyrite can be effectively depressed and separated from molybdenite using the combined method.

3.4 XPS analysis

The floatability of chalcopyrite and molybdenite is directly related to the degree of surface oxidation and the products obtained, which can be determined via XPS analysis. The XPS results are presented in Tables 2 and 3 and Figs. 8 and 9.

The high-resolution spectra of Cu $2p_{3/2}$, Fe 2p, and S 2p for chalcopyrite and the corresponding decoupling results are presented in Figs. 8 and Table 2. The Cu 2p peaks centered at about 932.14 eV and 933.59 eV could be assigned to Cu(I)−S and Cu(II)−O/OH, respectively [36,37]. The unsatisfactory floatability of chalcopyrite after oxidation could be attributed to the decrease in hydrophobic Cu(I)−S and the increase in hydrophilic Cu(II)−O/OH. For the untreated chalcopyrite, the content of Cu(II)−O/OH was 19.42%, indicating that the surface of chalcopyrite was oxidized prior to the pretreatment, which was inevitable as it was exposed to air. After single treatment with microwave or H_2O_2, the content of Cu(II)−O/OH increased to 35.58% and 33.82%, respectively, which contributed to the decrease in the floatability of chalcopyrite. However, after treatment with the combined oxidation method, the content of Cu(II)−O/OH increased significantly

Table 2 Quantification of chalcopyrite after different pretreatments based on Fig. 8

Element	Species	Untreated		H_2O_2		Microwave		Microwave+H_2O_2	
		B.E./eV	Content/ at.%	B.E./eV	Content/ at.%	B.E./eV	Content/ at.%	B.E./eV	Content/ at.%
Cu	Cu(I)−S	932.14	80.58	931.97	66.18	932.20	64.42	932.20	56.17
	Cu(II)−O/OH	933.59	19.42	932.97	33.82	933.30	35.58	932.97	43.83
Fe	Fe(II)−S	708.14	44.30	708.15	21.67	708.28	11.38	708.08	8.10
	Fe(III)−O/OH	711.32	43.82	711.35	64.93	711.0	69.43	710.95	73.82
	Fe(III)−SO_4^{2-}	713.50	11.80	713.55	13.36	713.30	19.19	713.33	18.08
S	S^{2-}	161.25/162.43	34.44	161.34/162.52	44.61	161.18/162.36	43.20	161.26/162.44	39.14
	S_2^{2-}	162.34/163.52	48.57	162.65/163.83	32.57	162.56/163.74	33.78	162.23/163.41	25.63
	S_n^{2-}/S^0	164.62/165.77	12.45	165.07/166.25	8.97	164.17/165.35	11.88	164.18/165.36	15.54
	SO_4^{2-}	168.05/169.23	4.55	168.55/169.73	13.85	168.63/169.81	11.14	168.66/169.84	19.68

Table 3 Quantification of molybdenite after different pretreatments based on Fig. 9

Element	Species	Untreated		H_2O_2		Microwave		Microwave+H_2O_2	
		B.E./eV	Content/ at.%	B.E./eV	Content/ at.%	B.E./eV	Content/ at.%	B.E./eV	Content/ at.%
Mo	MoS_2	229.72/232.84	93.04	229.86/232.98	91.48	229.67/232.79	91.23	229.76/232.88	89.14
	Mo−O	229.06/232.18	6.96	228.87/231.99	8.52	228.75/231.62	8.77	228.88/232.00	10.86
S	MoS_2	161.99/163.17	100	161.91/163.09	100	161.88/163.06	100	162.01/163.19	100

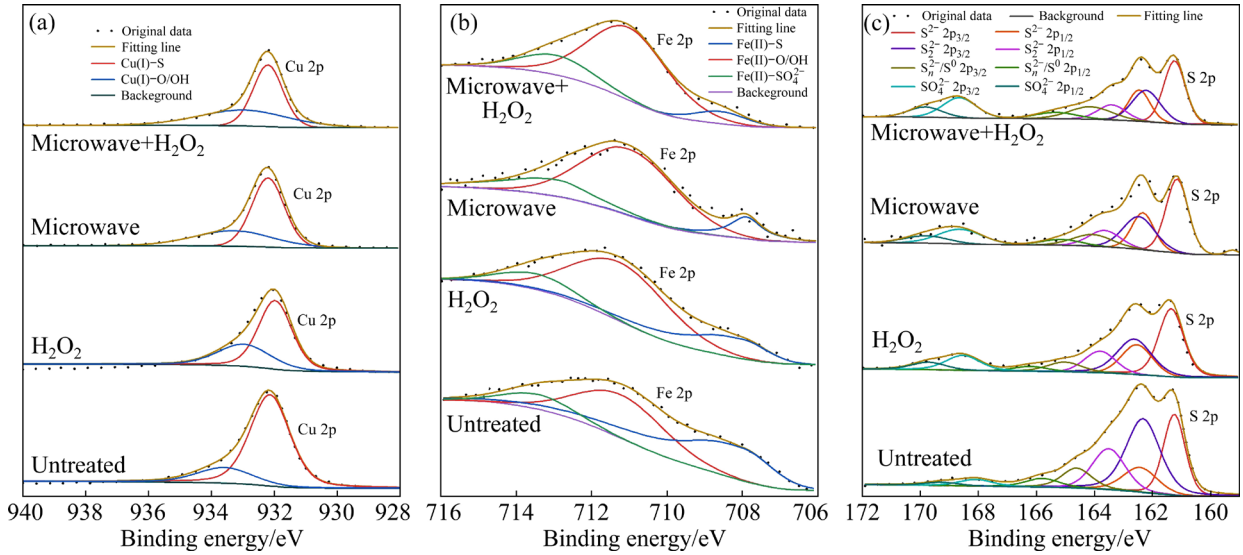

Fig. 8 Fitting peaks of Cu 2p (a), Fe 2p (b) and S 2p (c) for chalcopyrite after different pretreatments (pH 10.0, microwave power 500W, H_2O_2 dosage 3.2×10^{-3} mol/L)

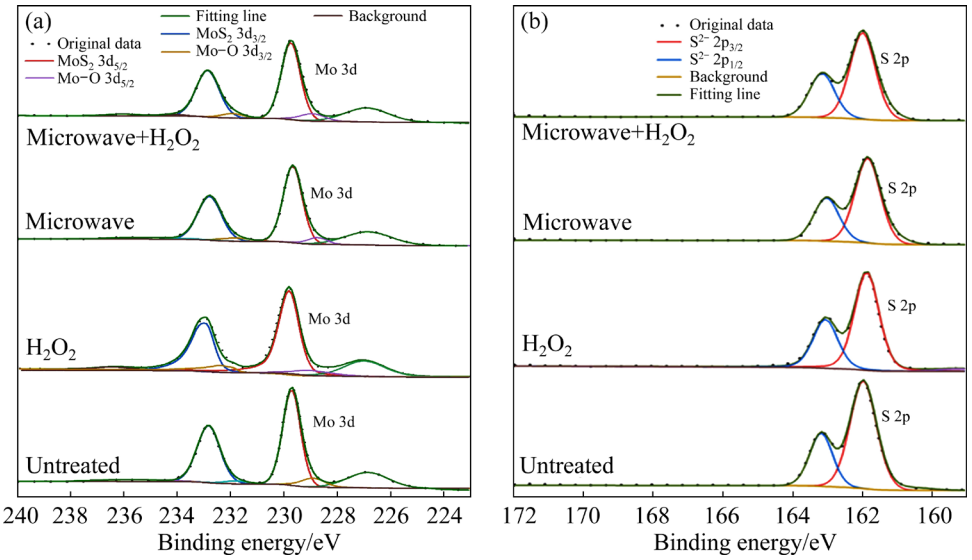

Fig. 9 Fitting peaks of Mo 3d (a) and S 2p (b) for molybdenite after different pretreatments (pH 10.0, microwave power 500W, H_2O_2 dosage 3.2×10^{-3} mol/L)

to 43.83%, thus indicating more intense oxidation compared with the single method.

The peaks centered at about 708 eV, 711 eV and 713 eV could be assigned to Fe(II)−S, Fe(III)−O/OH, and Fe(III)−SO_4^{2-}, respectively [38,39]. For the untreated chalcopyrite, the content of hydrophilic ferric oxides, such as $Fe(OH)_3$, and $Fe_2(SO_4)_3$, was 55.62 at.%. However, after oxidation, the number of hydrophilic species increased significantly. In particular, for the combined pretreatment, the content of ferric oxide reached 91.90%, whereas the content of hydrophobic Fe(II)−S was only 8.10%. This is another reason contributing to the weak floatability of chalcopyrite treated with the combined oxidation method. Additionally, a comparison of the decoupling results of Cu 2p showed that iron oxidation had likely occurred on the surface of chalcopyrite [40].

Figure 8(c) shows the high-resolution spectra of the S 2p peak fitting of chalcopyrite with and without pretreatment using the single microwave, H_2O_2 and combined oxidation methods. The S 2p peaks at approximately 161.40/162.58 eV, 162.9/164.08 eV, 164.20/165.26 eV, and 168.80/169.98 eV corresponded

to monosulfides, disulfides, polysulfides/elemental sulfur, and sulfates, respectively [41]. Among them, the S_2^{2-} and S_n^{2-}/S^0 species contributed positively to the surface hydrophobicity of chalcopyrite under different conditions [42]. In particular, the hydrophobicity of the S_n^{2-}/S^0 species was extremely strong. As shown in Table 2, the amount of S_2^{2-} and S_n^{2-}/S^0 species on the chalcopyrite surface without oxidation was 41.54%, whereas that of the hydrophilic sulfate species was only 2.82%. However, after oxidation pretreatment, the content of S_2^{2-}, S_n^{2-}/S^0 and sulfate species increased to different degrees. In particular, after the microwave pretreatment, the content of S_2^{2-} and S_n^{2-}/S^0 species reached 58.54%, which was the highest among the results with the different oxidation methods. Combining these findings with the fitting results of Cu 2p and Fe 2p, one can infer that the oxidation intensity of microwave irradiation at 500 W is stronger than that of H_2O_2 (3.2×10^{-3} mol/L), whereas the oxidation property is weaker owing to the higher amounts of hydrophobic S_2^{2-} and S_n^{2-}/S^0 species generated on the surface. This is consistent with the microflotation results shown in Fig. 2. For the combined oxidation, the amount of S_2^{2-} and S_n^{2-}/S^0 species was high. However, the amounts of hydrophilic copper, ferric oxides/hydroxides, and sulfates were extremely high, which resulted in the lowest surface contact angle and weakest flotation of chalcopyrite, as shown in Figs. 2−6.

The high-resolution spectra of Mo 3d and S 2p for molybdenite after different treatments and the corresponding decoupling results are shown in Figs. 9(a, b) and Table 3. For molybdenite, the peaks of Mo 3d centered at approximately 226.8 eV, 229.72 eV and 232.84 eV were assigned to S 2s, Mo $3d_{5/2}$, and Mo $3d_{3/2}$ of MoS_2, respectively [43]. The peaks of Mo 3d centered at approximately 229.06 eV and 232.18 eV were assigned to Mo $3d_{5/2}$ and Mo $3d_{3/2}$ of Mo−O, respectively. Prior to the pretreatments, only 6.96% of Mo−O species was generated on the surface due to autoxidation during the preparation. However, after the single and combined oxidation pretreatments, the amount of molybdenum oxides increased slightly, and the content of MoS_2 remained above 89%. As for the peaks of S 2p, only those of MoS_2 at about 161.99 eV and 163.17 eV were indicated in both cases with and without pretreatment. In fact, surface oxidation of molybdenite might have occurred under alkaline conditions and generated sulfates and Mo−O species such as MoO_3 and MoO_2. However, sulfates are dissoluble, and Mo−O species can be changed to dissoluble MoO_4^{2-} under the action of OH^- [44]. Therefore, for molybdenite, oxidation by the combined method was weak and minimally affected its surface hydrophobicity and floatability under alkaline conditions.

In conclusion, molybdenite exhibits stronger antioxidant properties than chalcopyrite. After treatment with single and combined oxidation pretreatments, only a scant amount of Mo−S on molybdenite surface was transformed to Mo−O, and the surface maintained its strong hydrophobicity. However, the surface of chalcopyrite was oxidized easily, which was primarily caused by the combined oxidation, and significant amounts of hydrophilic copper, ferric oxides/hydroxides and sulfates were generated on the surface. Therefore, the selective flotation separation of chalcopyrite and molybdenite can be achieved by combining microwaves and H_2O_2.

3.5 SEM analysis

To investigate the changes in the surface morphology of chalcopyrite and molybdenite after different pretreatments, SEM analysis was carried out. For the untreated chalcopyrite, its surface was flat and smooth, and no clear oxidation products were generated on the surface (see Fig. 10(a)). After single treatment with microwave power or H_2O_2, the surface topography changed slightly, indicating the weak oxidation effect of the single method. In addition, the edges of most of the chalcopyrite particles after treatment with H_2O_2 were rougher than those after microwave treatment, as shown in Fig. 10(b). This was caused by the corrosive effect of H_2O_2, as reported in the previous studies [45,46]. However, after treatment with the combined oxidation pretreatment, as shown in Fig. 10(d), the surface was relatively rough, and significant amounts of fine-sized oxidation products were generated on the surface. These fine particles were primarily attached to copper and ferric oxide floccules, which recrystallized to aggregate into acicular crystals of copper and ferric oxides [47]. In addition, these generated oxidation products could not be detached easily from the surface owing to the stirring action and the effect chemicals during flotation [48,49].

For molybdenite, the surface topography changed slightly with or without oxidation pretreatment using either the single or combined method (Fig. 11), indicating that its surface cannot be oxidized easily. This is because more non-polar and antioxidative surfaces, as shown in Figs. 11(b−d), were exposed to coarse molybdenite particles during sample preparation. Additionally, the surface of molybdenite was significantly rougher than that of chalcopyrite after different pretreatments, which was

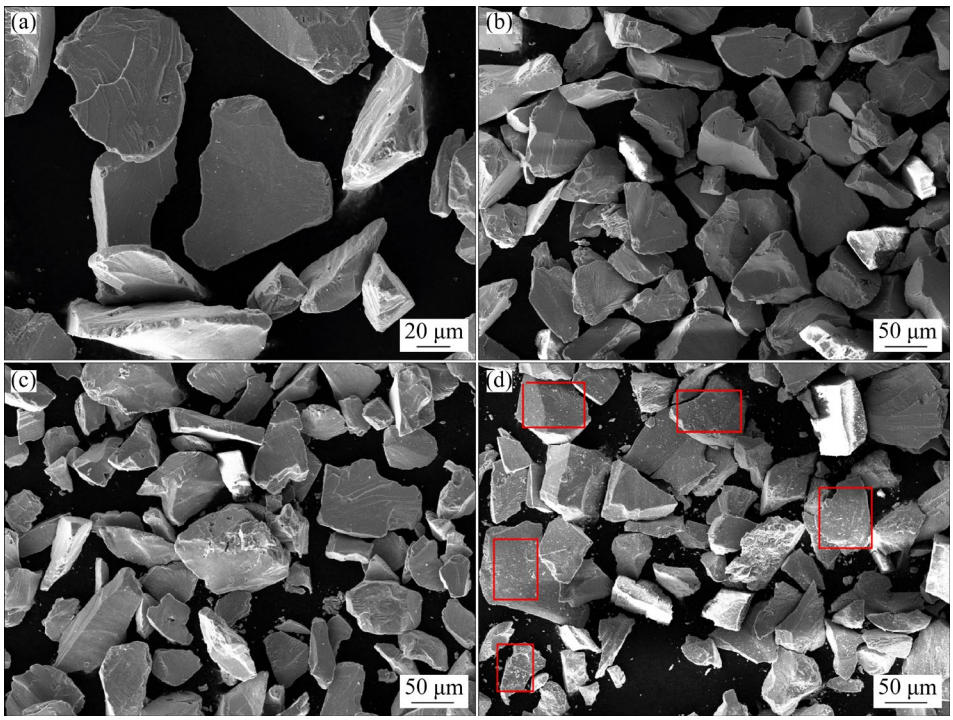

Fig. 10 Surface topographies of chalcopyrite after different pretreatments: (a) Untreated; (b) H_2O_2; (c) Microwave; (d) Microwave+H_2O_2

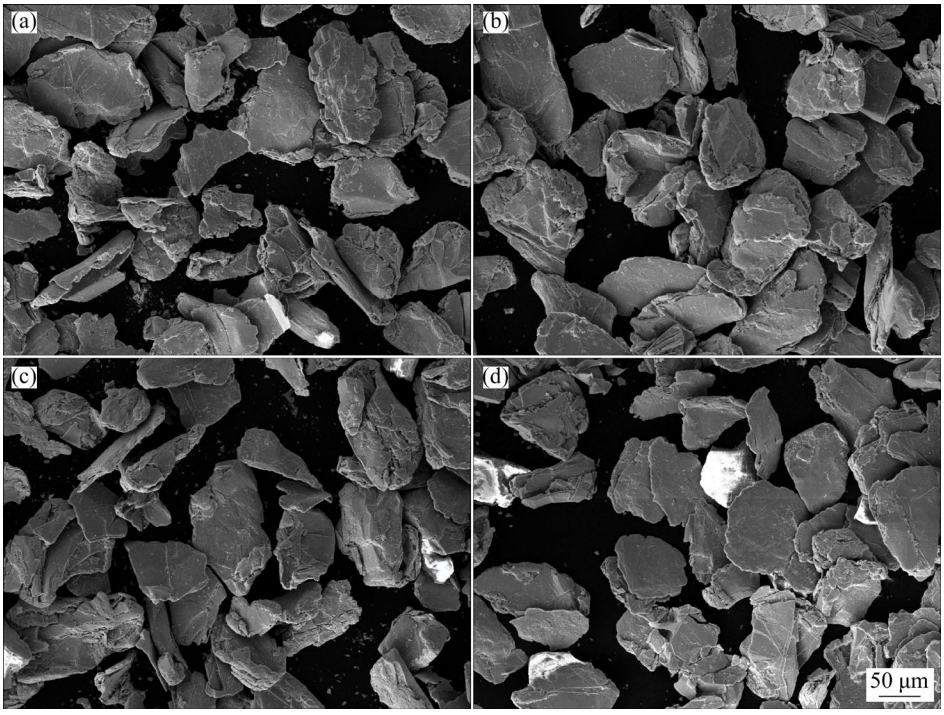

Fig. 11 Surface topographies of molybdenite after different pretreatments: (a) Untreated; (b) H_2O_2; (c) Microwave; (d) Microwave+H_2O_2

due to the grindability of the samples. Molybdenite is a layered mineral with a soft texture. Under the action of mechanical force, it is susceptible to fracture along the layer surface with weak molecular bonds and forms thin and flexible flakes [50], further increasing the difficulty of crushing and grinding.

3.6 AFM analysis

AFM is widely performed to obtain high-resolution measurement of the roughness of sample surface micro-areas owing to its advantages of high resolution, non-contact and three-dimensional surface descriptive properties. In this study, the morphologies of a 5 μm × 5 μm region on the surfaces of chalcopyrite and molybdenite undergoing various pretreatments were captured, and the results are shown in Figs. 12 and 13. The surface roughness parameters are listed in Table 4.

For the chalcopyrite sample not subjected to oxidation, its surface was generally smooth and no clear bumps and dents were observed, except for the scratch that was generated from polishing during sample preparation (Fig. 12(a)). After treatment with the single method, as shown in Figs. 12(b) and (c), clear peaks and valleys appeared in specific areas on the surface. The average R_a values after treatment with microwave and H_2O_2 were 32.2 nm and 35.9 nm, respectively. This indicated that the oxidation pretreatment increased the surface roughness due to the generation of copper, ferric oxides/hydroxides and sulfates on the surface. The surface roughness after treatment with H_2O_2 was higher than that after treatment with microwave, which was attributable to the erosion effect of H_2O_2. However, after treatment with the combined method, as shown in Fig. 12(d), more peaks and valleys appeared over the entire area, and the average surface roughness increased significantly to 61.5 nm. The role of surface roughness in the minerals flotation, such as malachite, magnesite, ilmenite and graphite, has been widely investigated [51−55]. An increase in surface roughness generally facilitates the adsorption of collectors, thereby improving the floatability of minerals. By contrast, the flotation of

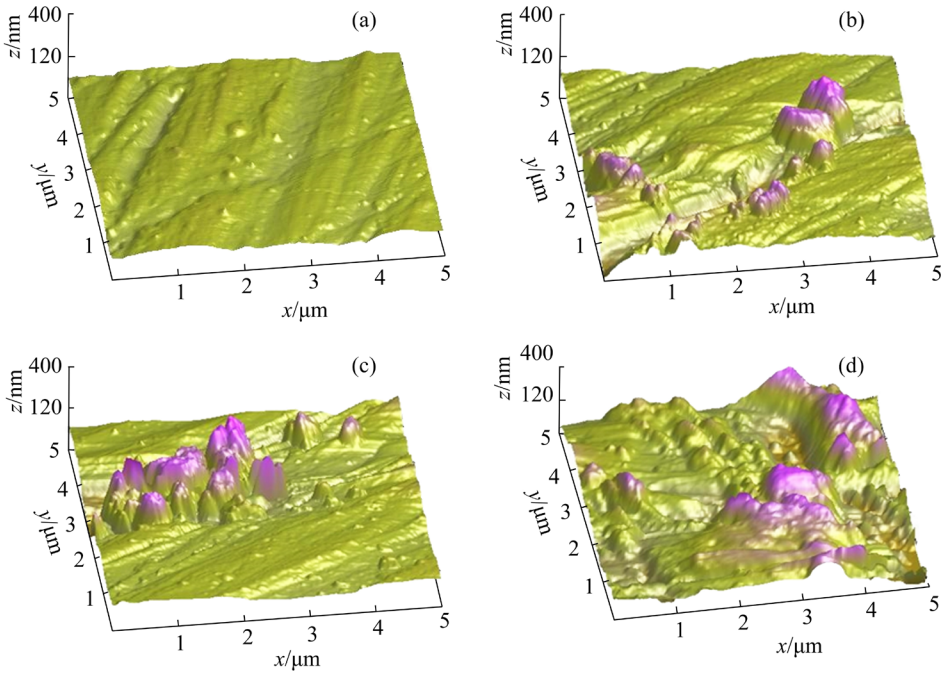

Fig. 12 AFM images of chalcopyrite after different treatments: (a) Untreated; (b) H_2O_2; (c) Microwave; (d) Microwave+H_2O_2

Table 4 Average surface roughness of chalcopyrite and molybdenite with different treatments

Sample	R_a/nm			
	Untreated	H_2O_2	Microwave	Microwave+H_2O_2
Chalcopyrite	14.7	35.9	32.2	61.5
Molybdenite	15.8	20	27.5	27.3

chalcopyrite showed the opposite trend as the surface roughness increased. This was because, after treatment with the single and combined methods, hydrophilic oxidation products were generated on the surface. These hydrophilic species decreased the surface hydrophobicity, as shown in Fig. 7, and weakened the adsorption of kerosene on the surface, thus consequently affecting the floatability of chalcopyrite, particularly after treatment with the combined method.

For the molybdenite sample not subjected to oxidation pretreatment, its surface was smooth and its roughness was similar to that of chalcopyrite (Fig. 13(a)). After treatment with the single and combined methods, the surface roughness increased to 20−27.3 nm, which was significantly lower than that of chalcopyrite treated with different methods. This indicated that only a few hydrophilic species, such as molybdenum oxides, were generated on the surface after oxidation. Therefore, the surface hydrophobicity and floatability decreased slightly compared with the case without oxidation pretreatment. In addition, the AFM results were contradictory to the SEM results, which showed that the surface of molybdenite was significantly rougher than that of chalcopyrite after different pretreatments. This was because the samples used for the AFM measurements were polished blocks.

3.7 Discussion

Molybdenite presents clear anisotropy, and two dissociation surfaces with entirely different properties are formed after crushing and grinding: nonpolar faces and polar edges. Nonpolar faces are formed owing to the rupture of the van der Waals forces between S−Mo−S layers and exhibit excellent hydrophobicity and antioxidative properties [34,35]. However, polar edges, which are relatively hydrophilic and easily oxidized, are derived from the cleavage of S−Mo covalent bonds. Therefore, the surface hydrophobicity of molybdenite is determined by the ratio of the edges and faces after crushing. For relatively coarse-grained molybdenite, nonpolar faces dominate. Therefore, molybdenite was difficult to oxidize even when using the combined oxidation method, and only a small amount of molybdenum oxide was generated on the surface after oxidation.

Chalcopyrite is a primary copper sulfide mineral that is more difficult to oxidize than other secondary copper sulfide minerals such as chalcocite. Therefore, the surface oxidation of chalcopyrite was weakened by the single microwave and H_2O_2 pretreatments, unless the oxidation intensity was increased. The surface wettability of chalcopyrite was primarily determined by the amounts of hydrophobic and hydrophilic species on its surface.

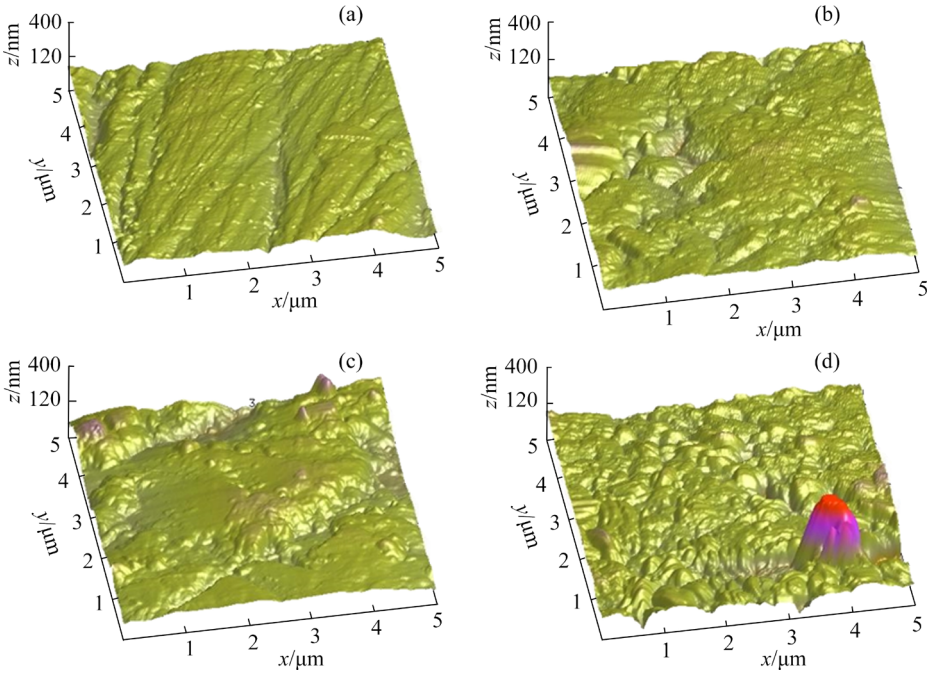

Fig. 13 AFM images of molybdenite after different treatments: (a) Untreated; (b) H_2O_2; (c) Microwave; (d) Microwave+ H_2O_2

After single treatment with microwave power or H_2O_2, the amounts of hydrophilic copper, ferric oxides/hydroxides, and sulfates on the surface increased, thus decreasing the surface hydrophobicity. Based on the XPS results that more oxidation products were generated on the chalcopyrite surface, one can infer that the oxidation intensity of the microwave pretreatment at 500 W was stronger than that of the H_2O_2 pretreatment (3.2×10^{-3} mol/L). However, the floatability and surface hydrophobicity of chalcopyrite after the microwave treatment were higher than those of chalcopyrite treated with H_2O_2. This was due to the higher amount of strongly hydrophobic S_2^{2-} and S_n^{2-}/S^0 generated on the surface.

Using the combined method, the effective depression of chalcopyrite in molybdenite flotation was achievable at a low microwave power and H_2O_2 dosage. Under the action of microwave, high-frequency charge transfer and ion conduction occurred inside the substance. The thermal motion of these molecules and the interaction between neighboring molecules produced effects similar to collision and friction, converting the electromagnetic energy lost in the entire process into internal energy, which is eventually released in the form of heat. During oxidation, microwaves can effectively and selectively transfer heat, intensify the vibration of polar molecules, and promote the overall heating of minerals, thus resulting in the surface oxidation of chalcopyrite. However, the formed oxidation layers are non-uniform, and further pretreatment in the H_2O_2 solution can compensate for this deficiency. In addition, after treatment with the combined method, the surface roughness of chalcopyrite increased significantly because significant amounts of fine-sized oxidation products were generated on the surface. Notably, Fe^{2+} and Fe^{3+} cations can induce the production of hydroxyl (·OH) and hydroperoxyl (·OOH) radicals from H_2O_2 via Fenton and Fenton-like reactions, respectively. However, these radicals are strong oxidizing agents under acidic conditions and easily lose their effectiveness under alkaline conditions.

Recently, other Fenton-like reactions using iron oxides (e.g., magnetite, goethite, and hematite) and $FeSO_4$ as catalysts have been shown to enhance the oxidation intensity of H_2O_2 under alkaline conditions [16]. These Fenton-like reactions are self-cyclic reactions, and Fe^{3+} from iron oxides can react with H_2O_2 to produce ·OOH/O_2 and Fe^{2+}, which can continue to react with H_2O_2 to generate iron oxides and ·OH. O_2 and other radicals can be generated via Fenton-like reactions under alkaline conditions, thereby improving the oxidation ability of H_2O_2. Therefore, it can be deduced that Fenton-like oxidation is dominant when using the combined method for the oxidation of chalcopyrite surface. Except for the formation of a uniform oxidation layer, the ferric oxides/hydroxides on the surface and the precipitates hydrolyzed from ferric ions in the solution further enhance the oxidation ability of H_2O_2 under alkaline conditions. A schematic of the surface oxidation mechanism of chalcopyrite and molybdenite with different pretreatments is presented in Fig. 14.

4 Conclusions

(1) The effective inhibition of chalcopyrite can be realized using combined oxidation pretreatments with low microwave power and H_2O_2 consumption. However, the flotation of molybdenite was not impeded by the use of the single or combined

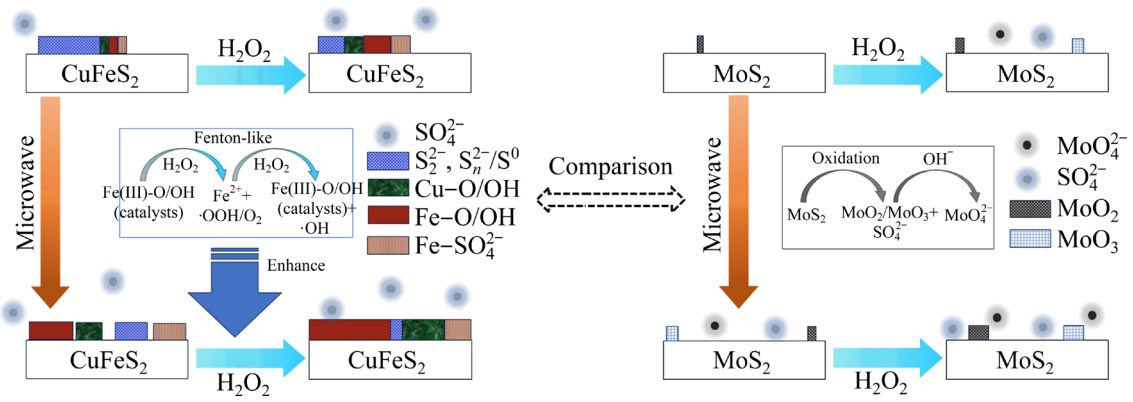

Fig. 14 Surface oxidation mechanism of chalcopyrite and molybdenite with different pretreatments

oxidation method. Therefore, chalcopyrite can be effectively separated from molybdenite using the combined oxidation method with microwaves and H_2O_2. High-quality molybdenum concentrates with a grade and recovery of 54.88% and 97.70%, respectively, were obtained under a microwave power of 500 W and a H_2O_2 dosage of 3.2×10^{-3} mol/L.

(2) For chalcopyrite, the oxidation intensity of microwaves (500 W) was stronger than that of H_2O_2 (3.2×10^{-3} mol/L). The content of hydrophilic oxidation products, such as copper and ferric oxides/hydroxides, generated on the surface after microwave pretreatment were significantly higher than that after pretreatment with H_2O_2. However, the generation of more hydrophobic S_2^{2-} and S_n^{2-}/S^0 species on the surface after microwave pretreatment weakened the inhibition effect on chalcopyrite flotation compared with the results after H_2O_2 pretreatment.

(3) After treatment with the combined oxidation method, more uniform oxidation products were generated on the chalcopyrite surface. In addition, the ferric oxides/hydroxides on the surface and the precipitates hydrolyzed from ferric ions in the solution served as catalysts, while O_2 and other radicals were generated via Fenton-like reactions, which further enhanced the oxidation power of H_2O_2 under alkaline conditions. The surface properties of molybdenite remained almost unchanged after treatment with either the single or combined method. Therefore, molybdenite maintained its excellent floatability after oxidation pretreatment.

CRediT authorship contribution statement

Ji-wei XUE: Data curation, Investigation, Methodology, Supervision, Writing – Original draft, Writing – Review & editing, Validation; **Qi-hong LIU:** Data curation, Investigation, Writing – Original draft; **Tong LIU:** Investigation, Formal analysis; **He WAN:** Methodology, Writing – Review & editing; **Sen WANG:** Conceptualization, Supervision, Writing – Review & editing. **Xian-zhong BU:** Data curation, Methodology, Project administration, Resources, Supervision, Writing – Review & editing, Validation.

Declaration of competing interest

The authors declare that they have no known competing financial interests or personal relationships that could have appeared to influence the work reported in this paper.

Acknowledgments

The authors gratefully acknowledge the financial support by the National Natural Science Foundation of China (Nos. 52104266, 52074206, 52374278), Key Research and Development Project of Shaanxi Province, China (No. 2023GXLH-054).

References

[1] YU Jin-sheng, LIU Run-qing, WANG Li, SUN Wei, PENG Hong, HU Yue-hua. Selective depression mechanism of ferric chromium lignin sulfonate for chalcopyrite–galena flotation separation [J]. International Journal of Minerals, Metallurgy and Materials, 2018, 25: 489−497.

[2] QIU Xue-min, YANG Hong-ying, CHEN Guo-bao, TONG Lin-lin, JIN Zhen-an, ZHANG Qin. Interface behavior of chalcopyrite during flotation from cyanide tailings [J]. International Journal of Minerals, Metallurgy and Materials, 2022, 29: 439−445.

[3] YANG Jing, CHEN Lu-zheng, XUE Zi-xing, YANG Kang-ning, SHAO Yan-hai, ZENG Jian-wu, GAO Yan-xiong. Performance evaluation of PHGMS technology for superfine chalcopyrite-molybdenite separation [J]. Separation and Purification Technology, 2024, 336: 126136.

[4] LASKOWSKI J S, CASTRO S, RAMOS O. Effect of seawater main components on frothability in the flotation of Cu−Mo sulfide ore [J]. Physicochemical Problems of Mineral Processing, 2014, 50: 17−29.

[5] SONG Shao-xian, ZHANG Xin-wang, YANG Bing-qiao, LOPEZ-MENDOZA A. Flotation of molybdenite fines as hydrophobic agglomerates [J]. Separation and Purification Technology, 2012, 98: 451−455.

[6] LIU Guang-yi, LU Yi-ping, ZHONG Hong, CAO Zhan-fang, XU Zhen-he. A novel approach for preferential flotation recovery of molybdenite from a porphyry copper–molybdenum ore [J]. Minerals Engineering, 2012, 36/37/38: 37−44.

[7] YIN Zhi-gang, SUN Wei, HU Yue-hua, ZHANG Chen-hu, GUAN Qing-jun, LIU Run-qing, CHEN Pan, TIAN Meng-jie. Utilization of acetic acid-[(hydrazinylthioxomethyl)thio]-sodium as a novel selective depressant for chalcopyrite in the flotation separation of molybdenite [J]. Separation and Purification Technology, 2017, 179: 248−256.

[8] HUANG Wei-xin, TANG Hong-hu, CAO Yang, LIU Ruo-hua, SUN Wei. Separation of molybdenite from chalcopyrite with thiolactic acid depressant: Flotation behavior and mechanism [J]. Transactions of Nonferrous Metals Society of China, 2023, 33: 3157−3167.

[9] ZHANG Xing-rong, JIANG Xin-yao, LUO An-ruo, CHEN Jian-hua, MENG Yao. A modified co-polyacrylamide to depress molybdenite in Cu/Mo separation and its competitive adsorption mechanism between reagents [J]. Separation and Purification Technology, 2024, 337: 126239.

[10] GUAN Chang-ping, YIN Zhi-gang, KHOSO S A, SUN Wei, HU Yue-hua. Performance analysis of thiocarbonohydrazide as a novel selective depressant for chalcopyrite in molybdenite-chalcopyrite separation [J]. Minerals, 2018, 8: 142.

[11] YANG Bing-qiao, YAN Hai, ZENG Meng-yuan, Zhu Han-yu.

Tiopronin as a novel copper depressant for the selective flotation separation of chalcopyrite and molybdenite [J]. Separation and Purification Technology, 2021, 266: 118576.

[12] YIN Zhi-gang, HU Yue-hua, SUN, Wei, ZHANG Chen-yang, HE Jian-yong, XU Zhi-jie, ZOU Jing-xiang, GUAN Chang-ping, ZHANG Chen-hu, GUAN Qing-jun, LIN Shang-yong, KHOSO S A. Adsorption mechanism of 4-amino-5-mercapto-1,2,4-triazole as flotation reagent on chalcopyrite [J]. Langmuir, 2018, 34: 4071−4083.

[13] YIN Zhi-gang, CHEN Sheng-da, XU Zhi-jie, ZHANG Chen-yang, HE Jian-yong, ZOU Jing-xiang, CHEN Dai-xiong, SUN Wei. Flotation separation of molybdenite from chalcopyrite using an environmentally-efficient depressant L-cysteine and its adsoption mechanism [J]. Minerals Engineering, 2020, 156: 106438.

[14] ZHONG Chun-hui, FENG Bo, WANG Hui-hui, CHEN Yuan-gan, GUO Meng-chi. The depression behavior and mechanism of tragacanth gum on chalcopyrite during Cu−Mo flotation separation [J]. Advanced Powder Technology, 2021, 32: 2712−2719.

[15] SUYANTARA G P W, HIRAJIMA T, MIKI H, SASAKI K, YAMANE M, TAKIDA E, KUROIWA S, IMAIZUMI Y. Effect of Fenton-like oxidation reagent on hydrophobicity and floatability of chalcopyrite and molybdenite [J]. Colloids and Surfaces A: Physicochemical and Engineering Aspects, 2018, 554: 34−48.

[16] SUYANTARA G P W, HIRAJIMA T, MIKI H, SASAKI K, YAMANE M, TAKIDA E, KUROIWA S, IMAIZUMI Y. Selective flotation of chalcopyrite and molybdenite using H_2O_2 oxidation method with the addition of ferrous sulfate [J]. Minerals Engineering, 2018, 122: 312−326.

[17] ZHANG Hong-tao, SONG Xiang-yu, HUANG Ye-hao, ZHANG Zhen, WANG Wen, XU Lai-fu. Selective flotation separation of molybdenite and chalcopyrite using O_3 oxidation method [J]. Transactions of Nonferrous Metals Society of China, 2024, 34: 298−308.

[18] MONTOYA A, REYES J L, REYES I A, CRUZ R, LAZARO I, RODRÍGUEZ I. Effect of sodium hypochlorite as a depressant for copper species in Cu−Mo flotation separation [J]. Minerals Engineering, 2023, 201: 108166.

[19] LIAO Run-peng, FENG Qi-chen, WEN Shu-ming, LIU Jian. Flotation separation of molybdenite from chalcopyrite using ferrate(VI) as selective depressant in the absence of a collector [J]. Minerals Engineering, 2020, 152: 106369.

[20] ZHENG Yong-xing, HUANG Yu-song, HU Pan-jin, QIU Xian-hui, LV Jin-fang, BAO Ling-yun. Flotation behaviors of chalcopyrite and galena using ferrate(VI) as a depressant [J]. International Journal of Mining Science and Technology, 2023, 33: 93−103.

[21] YANG Chao, JIN Xin, GUO Kun, DIAO Yue, JIN Peng-kang. Simultaneous removal of organics and ammonia using a novel composite magnetic anode in the electro-hybrid ozonation-coagulation (E-HOC) process toward leachate treatment [J]. Journal of Hazardous Materials, 2022, 439: 129664.

[22] HIRAJIMA T, MIKI H , SUYANTARA G P W, MATSUOKA H, ELMAHDY A M, SASAKI K, IMAIZUMI Y, KUROIWA S. Selective flotation of chalcopyrite and molybdenite with H_2O_2 oxidation [J]. Minerals Engineering, 2017, 100: 83−92.

[23] SILVA G R, WATERS K E. The effects of microwave irradiation on the floatability of chalcopyrite, pentlandite and pyrrhotite [J]. Advanced Powder Technology, 2018, 29: 3049−3061.

[24] HENDA R, HERMAS A, GEDYE R, ISLAMC M R. Microwave enhanced recovery of nickel-copper ore: Communition and floatability aspects [J]. Journal of Microwave Power and Electromagnetic Energy, 2005, 40: 7−16.

[25] XIE Xian, LI Bo-qi, XIE Rui-qi, TONG Xiong, LI Yue, ZHANG Shou-xun, LI Jia-wen, SONG Qiang. Al^{3+} enhanced the depressant of guar gum on the flotation separation of smithsonite from calcite [J]. Journal of Molecular Liquids, 2022, 368: 120759.

[26] LIAO Run-peng, HU Pan-jin, WEN Shu-ming, ZHENG Yong-xing, QIU Xian-hui, LÜ Jin-fang, LIU Jian. Interaction mechanism of ferrate(VI) with arsenopyrite surface and its effect on flotation separation of chalcopyrite from arsenopyrite [J]. Transactions of Nonferrous Metals Society of China, 2022, 32: 3731−3743.

[27] SUYANTARA G P W, HIRAJIMA T, ELMAHDY A M, MIKI H, SASAKI K. Effect of kerosene emulsion in $MgCl_2$ solution on the kinetics of bubble interactions with molybdenite and chalcopyrite [J]. Colloids and Surfaces A: Physicochemical and Engineering Aspects, 2016, 501: 98−113.

[28] ZHU Zhang-lei, YIN Wan-zhong, WANG Dong-hui, SUN Hao-ran, CHEN Ke-qiang, YANG Bin. The role of surface roughness in the wettability and floatability of quartz particles [J]. Applied Surface Science, 2020, 527: 146799.

[29] FUERSTENAU M C, SABACKY B J. On the natural floatability of sulfides [J]. International Journal of Mineral Processing, 1981, 8: 79−84.

[30] LUCAY F, CISTERNAS L A, GÁLVEZ E D, LÓPEZ-VALDIVIESO A. Study of the natural floatability of molybdenite fines in saline solutions and effect of gypsum precipitation [J]. Minerals & Metallurgical Processing, 2015, 32: 203−208.

[31] TODD E C, SHERMAN D M, PURTON J A. Surface oxidation of chalcopyrite ($CuFeS_2$) under ambient atmospheric and aqueous (pH 2−10) conditions: Cu, Fe L- and O K-edge X-ray spectroscopy [J]. Geochimica et Cosmochimica Acta, 2003, 67: 2137−2146.

[32] NICOLL W D, SMITH A F. Stability of dilute alkaline solutions of hydrogen peroxide [J]. Industrial & Engineering Chemistry, 1955, 47(12): 2548−2554.

[33] WEI Qian, JIAO Fen, DONG Liu-yang, LIU Xue-duan, QIN Wen-qing. Selective depression of copper-activated sphalerite by polyaspartic acid during chalcopyrite flotation [J]. Transactions of Nonferrous Metals Society of China, 2021, 31: 1784−1795.

[34] WANG Jing-yi, XIE Lei, LU Qing-ye, WANG Xiao-gang, WANG Jian-mei, ZENG Hong-bo. Electrochemical investigation of the interactions of organic and inorganic depressants on basal and edge planes of molybdenite [J]. Journal of Colloid and Interface Science, 2020, 570: 350−361.

[35] MIKI H, MATSUOKA H, HIRAJIMA T, SUYANTARA G P W, SASAKI K. Electrolysis oxidation of chalcopyrite and molybdenite for selective flotation [J]. Materials Transactions, 2017, 58: 761−767.

[36] DONG Jing-shen, LIU Quan-jun, YU Li, SUBHONQULOV S H. The interaction mechanism of Fe^{3+} and NH^{4+} on chalcopyrite surface and its response to flotation separation of

chalcopyrite from arsenopyrite [J]. Separation and Purification Technology, 2021, 256: 117778.
[37] MOIMANE T, HUAI Yang-yang, PENG Yong-jun. The critical degree of bornite surface oxidation in flotation [J]. Minerals Engineering, 2020, 155: 106445.
[38] DONG Wen-chao, LIU Run-qing, WANG Chang-tao, CAO Zheng-qiang, SUN Wei. Exact separation of sphalerite and pyrite by ferrophilic inhibitors in the EX-Cu(II) system: Interfacial adsorption and reactivity [J]. Transactions of Nonferrous Metals Society of China, 2024.
[39] TIAN Meng-jie, LIU Run-qing, GAO Zhi-yong, CHEN Pan, HAN Hai-sheng, WANG Li, ZHANG Chen-yang, SUN Wei, HU Yue-hua. Activation mechanism of Fe (III) ions in cassiterite flotation with benzohydroxamic acid collector [J]. Minerals Engineering, 2018, 119: 31−37.
[40] FAIRTHORNE G, FORNASIERO D, RALSTON J. Effect of oxidation on the collectorless flotation of chalcopyrite [J]. International Journal of Mineral Processing, 1997, 49: 31−48.
[41] SHEN Zhi-hao, WEN Shu-ming, HAO Jia-mei, FENG Qi-cheng. Flotation separation of chalcopyrite from pyrite using mineral fulvic acid as a selective depressant under weakly alkaline conditions [J]. Transactions of Nonferrous Metals Society of China, 2025, 35(1): 313−325.
[42] FENG Qi-Cheng, ZHAO Wen-juan, WEN Shu-ming, CAO Qin-bo. Copper sulfide species formed on malachite surfaces in relation to flotation [J]. Journal of Industrial and Engineering Chemistry, 2017, 48: 125−132.
[43] ZHONG Chun-hui, FENG Bo, CHEN Yuan-gan, GUO Meng-chi, WANG Hui-hui. Flotation separation of molybdenite and talc using tragacanth gum as depressant and potassium butyl xanthate as collector [J]. Transactions of Nonferrous Metals Society of China, 2021, 31: 3879−3890.
[44] BAKER M A, GILMORE R, LENARDI C, GISSLER W. XPS investigation of preferential sputtering of S from MoS_2 and determination of MoS_x stoichiometry from Mo and S peak positions [J]. Applied Surface Science, 1999, 150: 255−262.
[45] LUO Qing-yun, SHI Qing, LIU De-zhi, LI Bin-bin, JIN Sai-zhen. Effect of deep oxidation of chalcopyrite on surface properties and flotation performance [J]. International Journal of Mining Science and Technology, 2022, 32: 907−914.
[46] KHOSO S A, HU Yue-hua, LV Fei, GAO Ya, LIU Run-qing, SUN Wei. Xanthate interaction and flotation separation of H_2O_2-treated chalcopyrite and pyrite [J]. Transactions of Nonferrous Metals Society of China, 2019, 29: 2604−2614.
[47] SMART R St C. Surface layers in base metal sulphide flotation [J]. Minerals Engineering, 1991, 4: 891−909.
[48] GREET C J, SMART R St C. The effect of size separation by cyclosizing and sedimentation/decantation on mineral surfaces [J]. Minerals Engineering, 1997, 10: 995−1011.
[49] YIN Wan-zhong, XUE Ji-wei, LI Dong, SUN Qian-yu, YAO Jin, HUANG Shi. Flotation of heavily oxidized pyrite in the presence of fine digenite particles [J]. Minerals Engineering, 2018, 115: 142−149.
[50] CASTRO S, L-VALDIVIESO A, LASKOWSKI J S. Review of the flotation of molybdenite. Part I: Surface properties and floatability [J]. International Journal of Mineral Processing, 2016, 148: 48−58.
[51] ZHU Zhang-lei, FU Ya-feng, YIN Wan-zhong, SUN Haoran, CHEN Ke-qiang, TANG Yuan, YANG Bin. Role of surface roughness in the magnesite flotation and its mechanism [J]. Particuology, 2022, 62: 63−70.
[52] GONG Xiu-feng, YAO Jin, YIN Wan-zhong, YIN Xue-ming, BAN Xiao-qi, WANG Yu-lian. Effect of acid corrosion on the surface roughness and floatability of magnesite and dolomite [J]. Green and Smart Mining Engineering, 2024, 1(1): 118−125.
[53] LI Zhi-li, RAO Feng, C-ARROYO M A, BEDOLLA-JACUINDE A, SONG Shao-xian. Comminution effect on surface roughness and flotation behavior of malachite particles [J]. Minerals Engineering, 2019, 132: 1−7.
[54] TONG Zhong-yun, LIU Lei, YUAN Zhi-tao, LIU Jiong-tian, LU Ji-wei, LI Li-xia. The effect of comminution on surface roughness and wettability of graphite particles and their relation with flotation [J]. Minerals Engineering, 2021, 169: 106959.
[55] DU Yu-sheng, MENG Qing-you, YUAN Zhi-tao, KLEIN B, LI Li-xia, LU Ji-wei. Effect of acid surface pretreatment on the floatability difference between ilmenite and titanaugite pre-absorbed by flotation reagents [J]. Applied Surface Science, 2023, 613: 156121.

采用微波和双氧水组合氧化实现辉钼矿浮选中黄铜矿的有效抑制

薛季玮，刘启鸿，刘 童，宛 鹤，王 森，卜显忠

西安建筑科技大学 资源工程学院，西安 710055

摘 要：通过浮选试验、Zeta 电位、接触角、X 射线光电子能谱(XPS)、扫描电镜(SEM)和原子力显微镜(AFM)分析，全面研究微波与双氧水(H_2O_2)组合氧化预处理对辉钼矿和黄铜矿浮选分离的影响及其作用机理。浮选试验结果表明，在较低的微波功率和 H_2O_2 用量条件下，采用组合氧化预处理可实现黄铜矿的有效抑制。Zeta 电位、接触角和 XPS 分析表明，不同条件下预处理的辉钼矿表面疏水性变化不大，而黄铜矿表面形成了大量亲水性氧化组分，从而降低了黄铜矿的表面疏水性和可浮性。此外，SEM 和 AFM 分析表明，黄铜矿表面形成了更均匀的氧化产物，进一步使其表面粗糙度明显增加。

关键词：辉钼矿；黄铜矿；浮选分离；组合氧化；表面粗糙度

(Edited by Bin-bin PENG)